Interaction between an Island and the Ventilated Thermocline: Implications for the Hawaiian Lee Countercurrent

BO QIU AND THEODORE S. DURLAND

Department of Oceanography, University of Hawaii at Manoa, Honolulu, Hawaii

ABSTRACT

The ventilated thermocline theory is adapted to include the interaction between an island and the wind-driven subtropical circulation. The primary goal is an understanding of the effect of this interaction on the Hawaiian Lee Countercurrent (HLCC), an eastward current crossing the Pacific west of Hawaii in the latitude band 18°–21°N. A two-and-one-half-layer model is used, with the model island located in midgyre and equatorward of the gyre center, simulating the Hawaiian Islands. The presence of the island creates two wakes. A transport wake directly west of the island is characterized by an alteration of the zonal transport caused by the diversion of the interior flow incident upon the east coast of the island into zonal jets extending westward from the northern and southern tips of the island. A potential vorticity (pv) wake embedded in the second-layer streamlines westward and equatorward of the island is characterized by an alteration of the ventilated pv signature and of the baroclinic nature of the flow. The effects of the two wakes combine for a significant impact on both the transport and the baroclinic structure of the modeled HLCC, indicating that effective modeling of the HLCC should include not only the forcing mechanism, but also the influence of the large-scale Sverdrup flow to the east as modified by the Hawaiian Islands. In particular, a zonal variation in baroclinic structure is predicted that is consistent with observations.

1. Introduction

The establishment of the ventilated thermocline theory by Luyten et al. (1983, hereinafter referred to as LPS) and the potential vorticity (pv) homogenization theory by Rhines and Young (1982) has laid a solid foundation for our understanding of the large-scale wind-driven ocean circulation. These two elegant and complementary theories were not only a triumph for theoretical physical oceanography, they also provided new impetus to interpret observed circulation features on more solid dynamical bases. LPS, Talley (1985), and De Szoeke (1987, hereinafter DS) demonstrated that the ventilated thermocline theory accurately predicts large-scale features in the North Atlantic, North Pacific, and South Pacific, respectively. The effect of New Zealand on the South Pacific circulation was addressed by DS, but in that case the island lay within the western shadow zone, and the lower layers west of the island were assumed to be motionless. When an island resides in the ventilated region and near the gyre center (as does Hawaii), the likelihood of motion in the lower layer(s) west of the island must be considered, and new assumptions

must be made to adapt the ventilated thermocline theory to the vicinity of the island.

Our effort to understand the interaction between the island and the ventilated thermocline is motivated by several recent studies describing circulation features observed in the lee of the Hawaiian Islands. By analyzing historical surface drifter data available for the Hawaiian waters, Qiu et al. (1997) and Lumpkin (1998) showed that a narrow eastward current, dubbed the Hawaiian Lee Countercurrent (HLCC), exists west of the island of Hawaii (the "Big Island") in the latitudinal band of 19°–20°N (see Fig. 5 in Qiu et al. 1997). Despite being a relatively weak zonal current with a mean surface velocity of about 15 cm s^{-1}, the HLCC is identifiable in climatological surface dynamic topography maps, such as that (Fig. 1) constructed by Kobashi and Kawamura (2001) through combining historical and more recent World Ocean Circulation Experiment (WOCE) hydrographic data. In the figure, the HLCC corresponds to the 19°–21°N band west of the Big Island where the surface dynamic height contours of 190–210 cm veer abruptly eastward. In contrast to the drifter data showing the HLCC to be confined zonally near the Hawaiian Islands from 158°W to 168°W, Fig. 1 reveals that the HLCC can be detected as an entity as far west as 160°E (see also Aoki et al. 2002).

Figure 2 shows the zonal ADCP velocity and hydrographic sections for the meridional WOCE transects P14

Corresponding author address: Dr. Bo Qiu, Dept. of Oceanography, University of Hawaii at Manoa, 1000 Pope Road, Honolulu, HI 96822.
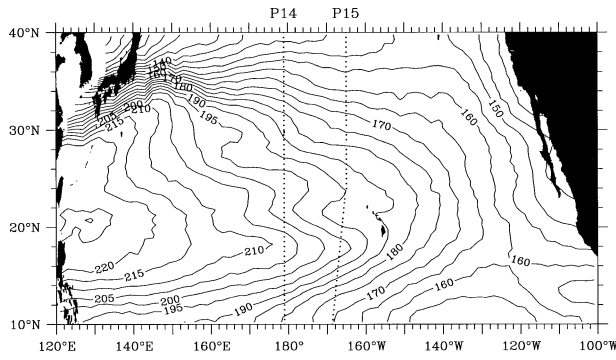E-mail: bo@soest.hawaii.edu

FIG. 1. Mean surface dynamic topography (cm) relative to 1000 dbar (adapted from Fig. 5a of Kobashi and Kawamura 2001). Dotted lines denote the two WOCE hydrographic/ADCP sections: P14 along 179°E and P15 along 165°W. Results from these two cruises are shown in Fig. 2.

and P15, both of which show eastward flow in the latitude band of the HLCC. WOCE P15 (Figs. 2a,b) is about 1100 km west of the Hawaiian Islands (Fig. 1), and it reveals an eastward flow between 17.5° and 20.5°N that is confined to the upper 150 m, with a maximum speed of 20 cm s^{-1}. WOCE P14 (Figs. 2c,d), about 2500 km west of the Hawaiian Islands, reveals a broader and deeper, but still surface-intensified eastward flow. Because the HLCC resides in a region of relatively

high eddy activity (Flament et al. 2001; Yu et al. 2002, manuscript submitted to *J. Phys. Oceanogr.*), any snapshot in time must be interpreted cautiously, and the exact significance of the above-mentioned eastward flows is open to debate. However, we show in section 4 that the difference in baroclinic structure of the eastward flow between Fig. 2a (P15) and Fig. 2c (P14) is consistent with the effect of the Hawaiian Islands on the ventilated Sverdrup flow from the northeast.

In pursuit of the forcing mechanism of the HLCC, Xie et al. (2001) analyzed surface wind measurements from the Quick Scatterometer (QuikSCAT) satellite and found the existence of intense positive and negative wind stress curl anomalies west and southwest of the Big Island, respectively. Under the forcing of these localized wind stress curl anomalies, they showed that an eastward zonal current similar to the observed HLCC and extending as far west as 130°E can be simulated in oceanic general circulation models of various dynamic complexity. Xie et al. (2001) emphasized the importance of this current to the coupled ocean–atmosphere system in that the advection of warm western Pacific surface water to the east generates a positive feedback that sustains the sea surface temperature and surface wind anomalies over the long distance between the Hawaiian Islands and the western boundary.

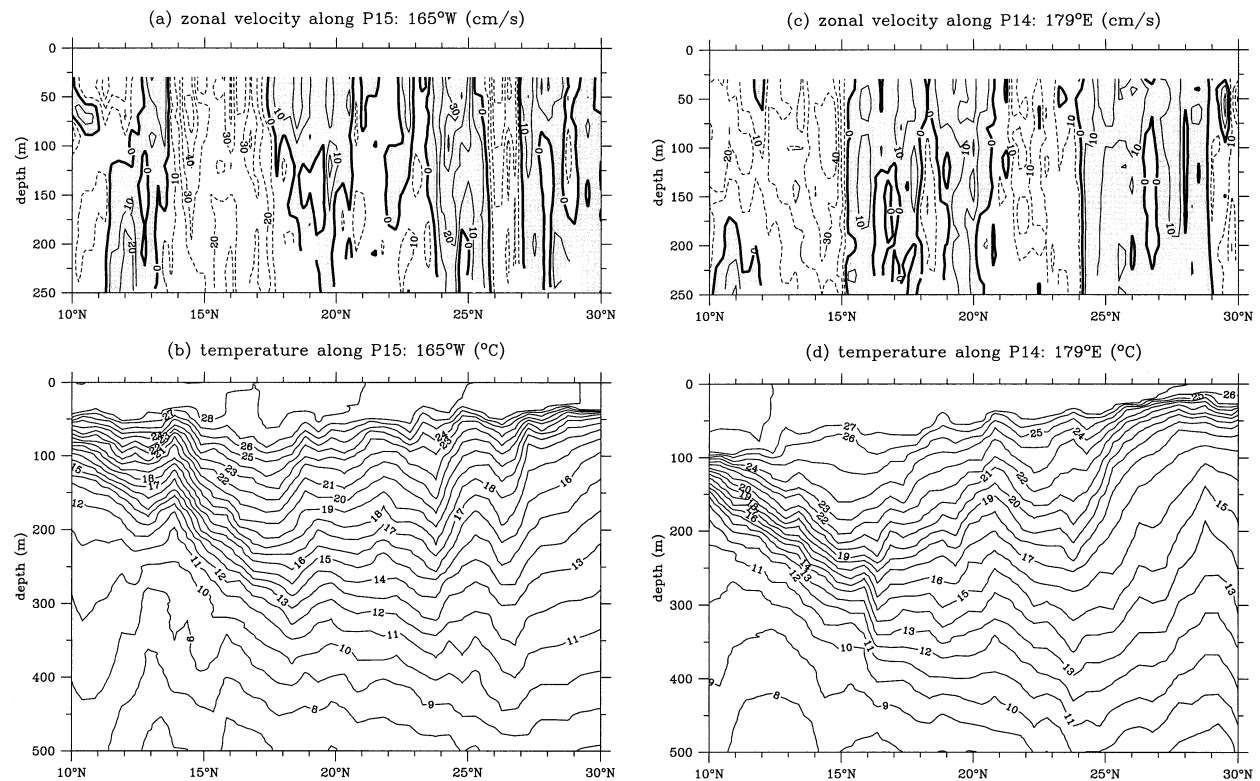Because the Hawaiian Islands exist in the middle of

FIG. 2. (a) Zonal velocity and (b) temperature distributions along 165°W from shipboard ADCP and CTD observations of the WOCE P15 cruise (Sep–Nov 1994). Shaded areas in (a) denote eastward flows. The same distributions along 179°E are shown in (c) and (d) based on the WOCE P14 cruise (Jul–Aug 1993). For more details of the P14 cruise, see Roden (1998).

the large-scale wind-driven subtropical gyre, detailed circulation patterns west of the Hawaiian Islands are influenced not only by the regional wind forcing, but also by the interior oceanic flow impinging upon the Hawaiian Islands from the east. Consequently, a complete understanding of the HLCC also requires an examination of how the islands interact with the interior circulation driven by the winds north and east of the islands. It is worth mentioning that the blocking of the barotropic interior transport by the Hawaiian Islands, and its influence upon the circulation to the west, was considered in an earlier study by White and Walker (1985). They assumed that all of the interior transport incident upon the east coast of the islands would turn north along this coast in a western boundary current. With the insight provided by Godfrey's (1989) island rule, we know in hindsight that this assumption is incorrect. Although it should accurately predict the influence on the barotropic transport directly west of the island chain, it would overestimate the influence on the zonal band extending west from the northern tip of the islands and miss the influence on the zonal band west of the southern tip.

In this study, we examine not only the blocking of the barotropic transport, but also the impact of the islands on the baroclinic nature of the flow, by adopting the two-and-one-half-layer ventilated thermocline model as our theoretical basis. In section 2 we develop the methodology to include an island in the LPS theory based on the lowest-order assumptions. Basically, these are 1) the assumption of Sverdrup dynamics everywhere except within an island western boundary current (wbc) and 2) some approximations based on the smallness of the island relative to the size of the gyre. In section 3 we apply this methodology to an idealized basin to clarify the effect of these assumptions on the flow west and southwest of the island. Section 4 employs a realistic basin geometry, island geometry, and wind forcing (including the above-mentioned dipole) and calculates the transport and baroclinic structure of the HLCC based on 1) the effect of the wind product alone and 2) the combined effect of the wind product and the perturbation of the general Sverdrup flow by the island. We show that the effect of the island on the ventilated thermocline flow is significant, particularly with regard to the baroclinic structure of the HLCC. In section 5, we address the effect of horizontal and vertical eddy diffusion upon the second-layer pv signal during the crossing of zonal jets produced by the island blocking effect. Results of the study are summarized in section 6.

2. Model

We consider a two-and-one-half-layer ventilated thermocline model of a Northern Hemisphere subtropical gyre, with major features shown in Fig. 3. An island resides in midgyre, well clear of the second-layer eastern shadow zone and western constant pv pool and south
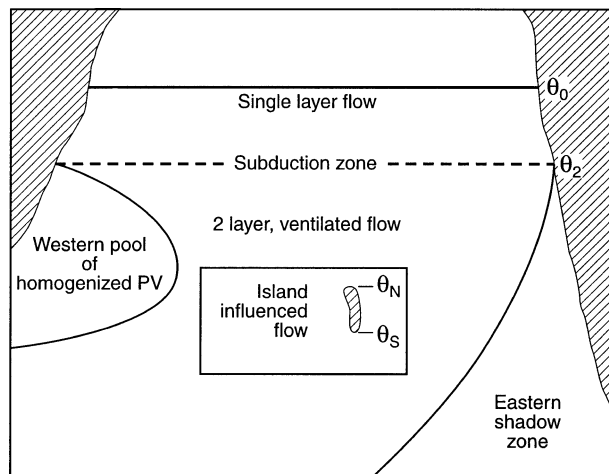

FIG. 3. Schematic of the two-and-one-half-layer ventilated thermocline model of the North Pacific Ocean.

of the gyre center, so that the Sverdrup flow impinges upon the island from the northeast. Our model basin and island are chosen to mimic the North Pacific and the major Hawaiian Islands, with the islands modeled as a continuous barrier. Qiu et al. (1997) have shown that this is a reasonable assumption with regard to the Hawaiian Islands. The meridional range of this barrier is small when compared with the gyre but is large enough so that deviations in the Coriolis parameter and in layer depths over this range are dynamically significant. Our model island has distinctive northernmost and southernmost points, and we refer to the entire coastline traveling clockwise (counterclockwise) from the northern tip to the southern tip as the east (west) coast.

Our methodology owes much to DS's treatment of New Zealand in a ventilated thermocline model of the South Pacific, but our assumptions regarding the region west of the island differ. He assumed that the lower layers were quiescent in this region, which, in the case of New Zealand, lies within the western shadow zone. We assume that in midgyre ventilated flow to the west of the island is probable. Because the ventilated thermocline theory is by now firmly established, we will assume familiarity with the fundamentals and present only the pertinent equations. In addition to the standard assumptions of ventilated thermocline theory, we must make some assumptions about the dynamics in the vicinity of the island. Our first is to assume that Sverdrup dynamics apply everywhere except in possible wbcs along the east coast of the island, and this has several immediate consequences, as follows.

- The possibility of eastern boundary currents and/or cross-isopycnal fluxes on the west coast of the island is not considered.
- Linear, inviscid flow along the west coast of the island is implied, allowing us to use Godfrey's (1989) island rule to determine the net transport between the island

and the eastern boundary. Qiu et al. (1997) have shown that this method accurately predicts important features of the circulation near the Hawaiian Islands.

- Imbalances between the net transport and the local value of the interior Sverdrup transport streamfunction along the east coast of the island force western boundary currents and, in general, result in pressure discontinuities between the island and the interior at the north and south tips of the island.
- Sverdrup dynamics west of the island result in the pressure discontinuities at the north and south tips being translated westward in zonal jets, which can be thought of as extensions of the island wbc.

Such zonal jets are ubiquitous in analytical analyses of Sverdrup flow interrupted by partial meridional boundaries (Pedlosky 1996, chapter 7) and are reported by Webb (2000) in a numerical model of the South Pacific, with some observational support (Webb 2000; Stanton et al. 2001). With the island in midgyre, the Sverdrup and second-layer transport streamlines will typically intersect these jets from the north, and continuity of the southward Sverdrup transport requires either that the second-layer flow cross the jet or that a diapycnal flux within the jet allows second-layer flow from the north to feed an increased first-layer flow to the south. We choose the first of these possibilities as the more reasonable one, because we are considering an island that is small relative to the gyre, and we do not anticipate overly energetic jets. It is clear that the jets do not consist merely of a zonal flow of the boundary current water, but rather are being constantly fed and depleted by the crossing of the interior flow, and this presents two issues that must be addressed in order to incorporate the influence of the island into the LPS theory:

1) how is the second-layer pv–pressure relationship of the interior water affected by the crossing of the jet, and
2) because crossing of the jets by the interior flow ensures that the wbc water must reenter the interior, how is the pv–pressure relationship of this water to be specified?

Our goal is to develop a model that illuminates the basic physics of the island-induced effects with a minimum of complexity, and, with this in mind, we approach item 1 by assuming that second-layer pv is conserved during the crossing of the jets. This is reasonable to expect if the island is small enough so that velocities and gradients within the jet are weak, and the only question is whether a model based on this assumption remains useful for the case of the Hawaiian Islands. In section 5, we estimate the pv change from vertical and horizontal eddy diffusion within the jet, assuming that this change represents a perturbation on the pv-conserving model using realistic winds and basin geometry. The relative change in pv induced by the jet crossing near the northern and southern tips of the Hawaiian

Islands is shown to be less than 8% and 5%, respectively, and this effect will decrease to the west as the jets widen and deepen. This small change justifies retaining the pv-conservation assumption, although we recognize that diffusive effects within the jets will introduce perturbations on the model results.

In the course of determining the interface depths at the island, we must make some assumptions about the island western boundary current structure. Depending again on the "smallness" of the island, we argue that it is reasonable to expect the horizontal velocity structures within the wbc to show a self similarity between layers. This expectation, combined with the assumption of pv conservation during the jet crossing, constrains the outflow regions of the northern and southern boundary currents to also exhibit a self similarity between layers, thus providing a pv–pressure relationship at these outflow regions (item 2).

Our notation and terminology follow LPS closely, with modifications and additions noted as we proceed. We denote H_n as the depth of the bottom of layer n. The layer-1 thickness is then $h_1 = H_1$, and the layer-2 thickness is $h_2 = H_2 - H_1$. We assume that the second layer outcrops at a constant latitude θ_2, where the Coriolis parameter takes the value f_2. The absence of alongshore winds at the eastern boundary leads to $H_1 = 0$ and $H_2 = H_{20}$, a constant, at the eastern boundary. At any point of the interior not directly west of the island,

$$\gamma_2 H_2^2(\phi, \theta) + \gamma_1 H_1^2(\phi, \theta) = \gamma_2[H_{20}^2 + D_0^2(\phi, \theta)], \quad (1)$$

where γ_n is the reduced gravity of layer n, $(\rho_{n+1} - \rho_n)g/\rho_0$, and

$$D_0^2 = \frac{-2f^2}{\beta\gamma_2} \int_\phi^{\phi_e(\theta)} w_E(\phi', \theta)R\cos\theta \, d\phi'. \quad (2)$$

The notation is standard. Directly west of the island,

$$\gamma_2 H_2^2(\phi, \theta) + \gamma_1 H_1^2(\phi, \theta)$$
$$= \gamma_2[H_{2i}^2(\theta) + D_{0i}^2(\phi, \theta)] + \gamma_1 H_{1i}^2(\theta), \quad (3)$$

where H_{1i} and H_{2i} denote the values of H_1 and H_2 along the west coast of the island, and

$$D_{0i}^2 = \frac{-2f^2}{\beta\gamma_2} \int_\phi^{\phi_{Iw}(\theta)} w_E(\phi', \theta)R\cos\theta \, d\phi'. \quad (4)$$

In the above, $\phi_e(\theta)$ is the longitude of the eastern boundary, and $\phi_{Iw}(\theta)$ is the longitude of the west coast of the island. In what follows, $\phi_{Ie}(\theta)$ is the longitude of the east coast of the island, θ_S and θ_N are the latitudes of the southern and northern extents of the island, and f_S and f_N are the values of the Coriolis parameter at these latitudes. In the ventilated regions north of θ_N or east of the island, the pv–pressure relationship set at the outcropping latitude yields

$$H_1 = (1 - f/f_2)H_2. \quad (5)$$

For regions west and southwest of the island, the pv–pressure relationship is to be determined. Although all

of the second-layer water in motion can be traced back to the ventilating region north of θ_2, in what follows we will reserve the term "ventilated" for water that retains the pv signature (5) of the subduction zone.

Because the regions north and east of the island are unaffected by the presence of the island, we concern ourselves with them only to the extent needed to determine the layer depths at the island and the transports of the island boundary currents. We begin with a somewhat general formulation, allowing for the possibility of alongshore winds at the island.

a. Island boundary currents

The first task is to determine the interface depths at the island, and in this we follow DS, with minor modifications for the different location of our island within the gyre and the addition of alongshore winds. Because only the first layer interacts directly with the Ekman layer, we will assume that an alongshore wind stress on the west coast of the island will be balanced by a pressure gradient in the first layer only. This corresponds to an onshore (offshore) geostrophic transport in the first layer balancing an offshore (onshore) Ekman transport in the mixed layer. The absence of a cross-shore transport in the second layer results in $H_{2i}(\theta) = H_{2I}$, a constant, along the west coast, a condition that extends to the south and north tips of the island. Labeling the first-layer thickness at the northern tip H_{1IN}, we have

$$H_{1i}^2(\theta) = H_{1IN}^2 + \frac{2}{\rho_0 \gamma_1} \int_{\theta_N}^{\theta} \boldsymbol{\tau} \cdot d\mathbf{l}, \qquad (6)$$

where H_{1i} is the variable first-layer thickness along the west coast, $\boldsymbol{\tau}$ is the vector wind stress, and the line integral is taken along the west coast from north to south, in keeping with the traditional island-rule integration direction.

One equation relating H_{1IN} and H_{2I} comes from noting that the net transport between the island and the eastern boundary is equal to the sum of the geostrophic and Ekman transports across any given latitude, $\theta_S \leq \theta \leq \theta_N$. Applying this equality at θ_N, we have

$$\gamma_2 H_{2I}^2 + \gamma_1 H_{1IN}^2 = \gamma_2 H_{20}^2 - 2f_N[T_{\mathrm{ir}} - T_E(\theta_N)], \quad (7)$$

where

$$T_{\mathrm{ir}} = \frac{1}{\rho_0(f_N - f_S)} \oint_{C_{\mathrm{ir}}} \boldsymbol{\tau} \cdot d\mathbf{l} \qquad (8)$$

is Godfrey's island rule for the net transport between the island and eastern boundary, and

$$T_E(\theta_N) = -\frac{1}{\rho_0 f_N} \int_{\phi_{Ie}(\theta_N)}^{\phi_e(\theta_N)} \tau^\phi R \cos\theta_N \, d\phi' \qquad (9)$$

is the net Ekman transport between the island and the eastern boundary across θ_N. In the above, τ^ϕ is the zonal component of $\boldsymbol{\tau}$, and C_{ir} is the standard counterclockwise island-rule contour encircling the island and extending

to the eastern boundary. Evaluating (7) at θ_S and using (6) to convert $H_{1i}^2(\theta_S)$ to H_{1IN}^2 gives a relationship between H_{1IN} and H_{2I} identical to that in (7).

The conservation of mass transport in layer 2 provides a second relationship between H_{1IN} and H_{2I}:

$$\int_{\phi_{Ie}(\theta_S)}^{\phi_e} (H_2 - H_1)\frac{\gamma_2}{f_S}\frac{\partial H_2}{\partial \phi} \, d\phi$$

$$= \int_{\phi_{Ie}(\theta_N)}^{\phi_e} (H_2 - H_1)\frac{\gamma_2}{f_N}\frac{\partial H_2}{\partial \phi} \, d\phi, \qquad (10)$$

where the lhs is the layer-2 transport between the island and the eastern boundary across θ_S, and the rhs is the corresponding transport across θ_N. By treating the boundary current and interior transports separately, this equation can be rearranged to give

$$\frac{1}{f_N} \int_{\phi_{Ie}(\theta_N)}^{\phi_{Ie}(\theta_N)+\delta} (H_2 - H_1)\frac{\partial H_2}{\partial \phi} \, d\phi$$

$$- \frac{1}{f_S} \int_{\phi_{Ie}(\theta_S)}^{\phi_{Ie}(\theta_S)+\delta} (H_2 - H_1)\frac{\partial H_2}{\partial \phi} \, d\phi$$

$$= \frac{1}{2f_2}(H_{2WN}^2 - H_{2WS}^2), \qquad (11)$$

where the subscript W appended to H_2 denotes the westernmost extent of the interior solution, just outside the island boundary current, and the additional subscript N or S denotes the latitude of the northern or southern island tip. The integrals represent the layer-2 boundary current transports at the north and south tips of the island, with δ being the boundary current width, and the integrated term represents the net transport from the layer-2 interior flow east of the island into the boundary current.

To evaluate the boundary current integrals, we need to make some assumptions about the boundary current structure. Because of the smallness of the island, we expect the dynamics to be dominantly linear in both layers [long-term mean current profiles of the northern branch of the boundary current, the North Hawaiian Ridge Current (NHRC), yield a Rossby number of 0.06]. Although vertical shear exists within the boundary current, we expect it to be relatively small, so that cross-isopycnal fluxes of mass and momentum are negligible. Given that the ocean gets deep rapidly off the Hawaiian coast, we expect the boundary current dynamics in both layers to be dominated by horizontal vorticity diffusion, leading to a self-similarity between the horizontal profiles of velocity in the two layers. This equivalent barotropic picture of the boundary current is supported by ADCP measurements across the NHRC (Qiu et al. 1997, their Fig. 3) and allows H_1 to be expressed as a linear function of H_2 within the boundary current (appendix A). In this case,

$$\int_{\phi_{Ie}(\theta_N)}^{\phi_{Ie}(\theta_N)+\delta} (H_2 - H_1)\frac{\partial H_2}{\partial \phi}\, d\phi$$

$$= (H_{2WN} - H_{2I})\frac{(H_{2WN} - H_{1WN}) + (H_{2I} - H_{1IN})}{2}, \quad (12)$$

with a similar expression for the southern integral. Using (12) to evaluate the second-layer wbc transports in (11) produces the second relation between H_{1IN} and H_{2I}:

$$H_{1IN} = H_{2I}\frac{f_N(H_{2I} - H_{1WS}) - f_S(H_{2I} - H_{1WN})}{R_H f_N(H_{2I} - H_{2WS}) - f_S(H_{2I} - H_{2WN})}, \quad (13)$$

where

$$R_H = \frac{H_{1i}(\theta_S)}{H_{1IN}} = \left(1 + \frac{2}{\rho_0 \gamma_1 H_{1IN}^2}\int_{\theta_N}^{\theta_S} \boldsymbol{\tau}\cdot d\mathbf{l}\right)^{1/2}. \quad (14)$$

The implicit relationship (13) must be solved numerically in conjunction with (7) to yield H_{1IN} and H_{2I}. When the effect of alongshore wind forcing on the west coast of the island is negligible, $H_{1i}(\theta) = H_{1IN}$ and $R_H = 1$.[1] In this case, (13) becomes an explicit expression for H_{1IN}, which, in conjunction with (7), yields a fourth-degree polynomial solution for H_{2I}.

b. Northern tip of island

We next look at conditions near the northern tip of the island. We have restricted ourselves to the case in which the Sverdrup transport streamlines approach from the northeast quadrant, and will further restrict ourselves to the case in which the layer-2 streamlines approach from the same quadrant. It is reasonable to expect this condition to follow from the first, given the beta spiral effect. Wajsowicz (1993) and Pedlosky et al. (1997) have shown that when the circulation of the wind stress around the island is small in comparison with the circulation around the traditional island-rule contour, the net island-rule transport T_{ir} is essentially the average of the Sverdrup transport streamfunction values along the east coast of the island. A monotonic decrease in the streamfunction from north to south, consistent with flow from the northeast, would then result in a northward wbc near the northern tip of the island. A strong-enough alongshore wind anomaly on the west coast of the island could conceivably reverse the wbc transport, but this is not true for Hawaii, and we will not consider that possibility here. With the layer-2 streamlines approaching from the northeast, the second-layer wbc transport near the northern tip of the island is also northward.

Figure 4 shows a schematic of the vicinity of the northern tip with impinging layer-2 streamlines. The wbc and zonal jet are shown with finite width, although
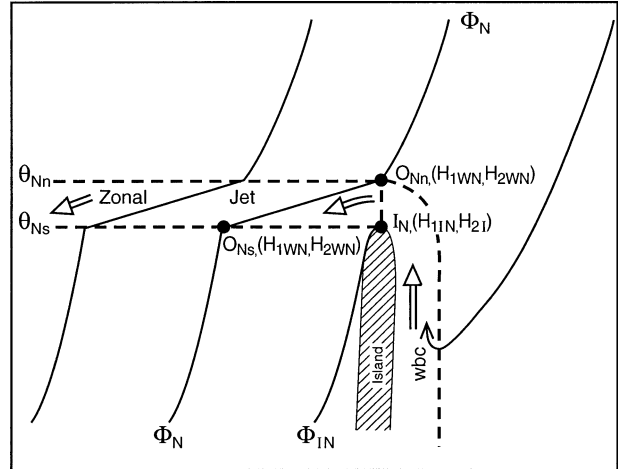
FIG. 4. Layer-2 streamlines near the northern tip of the island: Φ_N denotes the critical streamline which passes through O_{Nn}, the transition point between the wbc and the zonal jet; Φ_N and streamlines to the northwest cross the jet, conserving pv. Streamlines to the southeast of Φ_N enter the wbc and lose the subduction-zone pv signature. Streamline Φ_{IN} originates at the northern tip of the island and borders the shadow zone adjacent to the island's west coast.

in the model they are represented by pressure discontinuities of infinitesimal width. The transect $I_N - O_{Nn}$, extending north from the tip of the island, separates the wbc regime to the southeast from the zonal jet regime to the west. The interface depths at points I_N and O_{Nn} are labeled as previously described for the northern tip of the island and the adjacent interior. Here, Φ_N is the layer-2 interior streamline that intersects the transition from wbc to zonal jet at O_{Nn}, and it divides the interior flow between two different fates. Because the second-layer wbc transport is northward near θ_N, Φ_N jogs to the west, from O_{Nn} to O_{Ns}, as it crosses the jet, and pv conservation across an infinitesimally thin zonal jet ensures that the interface depths remain unchanged during the crossing. All streamlines west of Φ_N likewise jog to the west at θ_N while conserving pv, and (5) holds for these streamlines. With (3) and (6), the solution for the region west of Φ_N, and between θ_S and θ_N, is fully determined.

Streamlines to the south and east of Φ_N enter the wbc, thus losing the pv signature carried from the subduction zone, and rejoin the interior flow in the boundary current outflow region between sections $I_N - O_{Nn}$ and $I_N - O_{Ns}$. Because this transition region is bounded by a pv-conserving streamline, conservation of mass transport between streamlines requires that the self similarity between layers assumed for the boundary current must also hold throughout the transition region, even though the dynamics change from boundary current to Sverdrup. In appendix B we show that this works for any arbitrary monotonic wbc and Sverdrup structure functions. The self-similarity requirement then gives a relationship between h_2 and H_2 at $I_N - O_{Ns}$:

$$h_2(\theta_N) = H_2 - H_1 = A_N H_2 + B_N, \qquad (15)$$

where

$$A_N = 1 - \frac{H_{1WN} - H_{1IN}}{H_{2WN} - H_{2I}}, \quad \text{and} \qquad (16)$$

$$B_N = \left(\frac{H_{1WN} - H_{1IN}}{H_{2WN} - H_{2I}}\right) H_{2WN} - H_{1WN}. \qquad (17)$$

Along streamlines originating from $I_N - O_{Ns}$, pv conservation then gives

$$H_1 = \left(1 - \frac{f}{f_N} A_N\right) H_2 - \frac{f}{f_N} B_N. \qquad (18)$$

Equations (18), (3), and (6) now yield a quadratic equation for H_2 along streamlines originating from the transect $I_N - O_{Ns}$, and the larger of the two roots is the appropriate one.

In the absence of alongshore winds on the west coast of the island, the pv-conserving streamline originating at I_N must pull away from the island and create a shadow zone completely equivalent to the shadow zone at the eastern boundary. We label this streamline Φ_{IN}, signifying its origin at the northern tip, and follow LPS in assuming that the lower layer is quiescent between this streamline and the island. Hence,

$$H_2(\phi, \theta) = H_{2I}, \qquad (19)$$

in conjunction with (3) and (6) constitutes the solution between Φ_{IN} and the island. The presence of alongshore winds on the west coast will affect the size of the shadow zone because of the variation in H_{1i} along the coast and could conceivably eliminate the shadow zone and create a more complicated dynamical situation near this coast. In the case of Hawaii, this effect is small [see footnote 1 and (14)], and it serves only to shift the location of the shadow zone boundary Φ_{IN}.

c. Southern tip of island

We now consider the situation near the southern tip of the island. Figure 5 shows a schematic of the critical streamlines near the island, and a labeling of the regions that they delineate. Here Φ_N, as discussed above, is an eastern boundary for the ventilated regions (labeled V) west and southwest of the island that retain the pv set at the subduction zone. The streamline Φ_{IN} is the eastern boundary for the region (B_N) where the pv is determined at the outflow of the northern wbc, and the western boundary for the island shadow zone (S). The additional subscript W is appended to a region or streamline label to indicate conditions west of the island where the integration from the island boundary condition completes the solution [(3)]. The subscript S denotes conditions southwest of the island, controlled by the eastern boundary condition as in (1). At the southern tip, the transition from wbc to zonal jet happens at the transect $I_S - O_{Se}$.
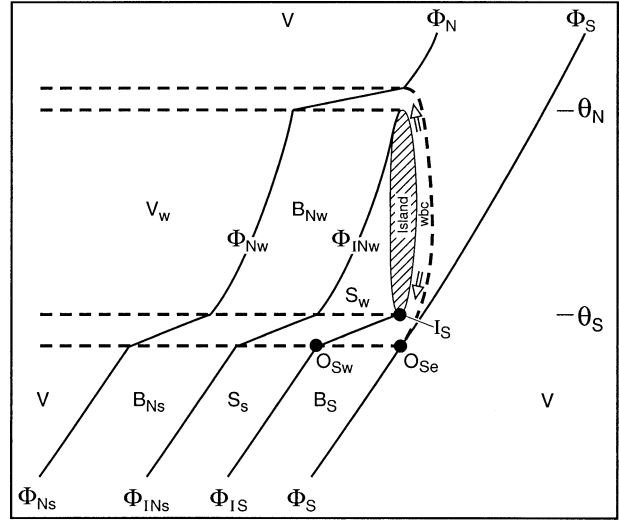

FIG. 5. Layer-2 streamlines bounding distinct dynamic regimes in the vicinity of the island: V, ventilated regions where the pv signature was determined at the subduction zone; B_N, regions where the pv signature was determined at the outflow of the northern wbc; S, island shadow zone where $H_2 = H_{2I}$; B_S, region where the pv signature was determined at the outflow of the southern wbc. The additional lower case subscripts w and s distinguish regions and streamline segments directly west of the island from those south of θ_S.

Here, Φ_S is the interior streamline that passes through O_{Se} and separates the flow to the northwest that enters the wbc and loses its pv signature from flow to the southeast that remains unaffected by the presence of the island.

The approach of the Sverdrup and second-layer streamlines from the northeast ensures that near the southern tip of the island the barotropic and layer-2 transport will be southward in the wbc and westward in the southern zonal jet. Because the second layer is quiescent in the shadow zone north of the southern jet, there can be no second-layer flow across the jet bordering this region. The first layer carries all of the Sverdrup flow across the jet, and the consequent pressure gradient in the first layer also rules out the possibility of a purely zonal, pv-conserving second-layer flow within this section of the jet. Consequently, the quiescent second-layer shadow zone is translated across the jet to the south with $H_2 = H_{2I}$, and there will be a pv-conserving streamline from the island tip through a point O_{Sw} on the southern boundary of the jet that bounds this region to the east. We label this streamline Φ_{IS} and, following the same logic used at the northern tip, deduce that the wbc water must flow southward across $O_{Sw} - O_{Se}$, distributed so as to satisfy the Sverdrup constraints. This flow leaves the transect $O_{Sw} - O_{Se}$ with $q_2 = f_S/h_2$, and at points farther south, pv conservation yields

$$H_1 = \left(1 - \frac{f}{f_S} A_S\right) H_2 - \frac{f}{f_S} B_S, \qquad (20)$$

where

$$A_S = 1 - \frac{H_{1WS} - H_{1i}(\theta_S)}{H_{2WS} - H_{2I}}, \quad \text{and} \quad (21)$$

$$B_S = \left[\frac{H_{1WS} - H_{1i}(\theta_S)}{H_{2WS} - H_{2I}}\right]H_{2WS} - H_{1WS}. \quad (22)$$

The region containing the outflow of the southern wbc is labeled B_S, and (1) and (6) complete the solution for this region. Again, the larger root in the quadratic equation for H_2 is the appropriate one.

Layer-2 flow in regions V_w and B_{Nw} is clearly from the north, and the bounding streamlines Φ_N and Φ_{IN} jog to the west in the crossing of the southern jet. The pv-conserving relations in the regions V, B_{Ns}, and S_s south of the jet are identical to the relations for the corresponding regions north of the jet.

d. Potential vorticity–conserving relationships and critical streamlines

We compile here the pv-conserving H_1–H_2 relationships for each of the dynamical regimes shown in Fig. 5:

$$V, V_w: \qquad H_1 = \left(1 - \frac{f}{f_2}\right)H_2, \qquad (23)$$

$$B_{Nw}, B_{Ns}: \qquad H_1 = \left(1 - \frac{f}{f_N}A_N\right)H_2 - \frac{f}{f_N}B_N, \quad (24)$$

$$S_w, S_s: \qquad H_2 = H_{2I}, \quad \text{and} \qquad (25)$$

$$B_S: \qquad H_1 = \left(1 - \frac{f}{f_S}A_S\right)H_2 - \frac{f}{f_S}B_S, \qquad (26)$$

where A_N, B_N and A_S, B_S are defined in (16), (17), and (21), (22), respectively; H_{1WN}, H_{2WN} and H_{1WS}, H_{2WS} are found by solving the interior equations, (1) and (5), at $[\phi_{Ie}(\theta_N), \theta_N]$ and $[\phi_{Ie}(\theta_S), \theta_S]$; H_{1IN} and H_{2I} are found by solving (7) and (13); and $H_{1i}(\theta)$ is given by (6).

Using the above equations, and the appropriate equation [(1) or (3)], implicit formulas for the bounding streamlines can be derived, and they are presented below:

$$\Phi_{Nw}: \qquad D_{0i}^2(\phi, \theta) = [1 + \Gamma_{12}(1 - f/f_2)^2]H_{2WN}^2 - H_{2I}^2 - \Gamma_{12}H_{1i}^2(\theta), \qquad (27)$$

$$\Phi_{Ns}: \qquad D_0^2(\phi, \theta) = [1 + \Gamma_{12}(1 - f/f_2)^2]H_{2WN}^2 - H_{20}^2, \qquad (28)$$

$$\Phi_{INw}: \qquad D_{0i}^2(\phi, \theta) = \Gamma_{12}[(1 - A_N f/f_N)H_{2I} - B_N f/f_N]^2 - \Gamma_{12}H_{1i}^2(\theta), \qquad (29)$$

$$\Phi_{INs}: \qquad D_0^2(\phi, \theta) = \Gamma_{12}[(1 - A_N f/f_N)H_{2I} - B_N f/f_N]^2 + H_{2I}^2 - H_{20}^2, \qquad (30)$$

$$\Phi_{IS}: \qquad D_0^2(\phi, \theta) = \Gamma_{12}[(1 - A_S f/f_S)H_{2I} - B_S f/f_S]^2 + H_{2I}^2 - H_{20}^2, \qquad (31)$$

$$\Phi_S: \qquad D_0^2(\phi, \theta) = [1 + \Gamma_{12}(1 - f/f_2)^2]H_{2WS}^2 - H_{20}^2, \qquad (32)$$

where $\Gamma_{12} = \gamma_1/\gamma_2$.

3. Application to an idealized ocean basin

We now look at the consequences of the model in a typical idealized rectangular basin with zonal winds. The wind stress varies sinusoidally with θ:

$$\tau^\phi = \tau_0 \sin[(\theta - \theta_c)\pi/W], \qquad (33)$$

and the values $\tau_0 = 0.08$ N m^{-2}, $\theta_c = 28.5°$N, and $W = 26°$ give an Ekman pumping distribution similar to that inferred for the North Pacific from ECMWF climatological winds. Other parameters relevant to the two-and-one-half-layer ventilated thermocline model are listed in Table 1. Figure 6 shows the model basin with the first- and second-layer isobars unperturbed by the presence of the island. The locations of two separate model islands, A and B, are superimposed on the isobars, with the southernmost (A) approximating the location of the Hawaiian Islands relative to the eastern boundary and the center of the gyre. The islands are

modeled as thin meridional barriers with lengths of 4° latitude.

a. Island A

Figure 7 shows the vicinity of island A, with the layer isobars perturbed by the island. The dynamical regimes discussed in the last section and shown in Fig. 5 are labeled here on the second-layer (lower) plot, and the regime boundaries are shown by dashed lines on each plot. The qualitative effect of the island on the Sverdrup flow directly west of the island and between the two zonal jets is expected. In the shadow zone, all of the flow is carried by the first layer, and it is predominantly southward because of the proximity to the island boundary. In the ventilated region V_w, the isobars in both layers are merely rotated counterclockwise from what they would have been in the absence of the island. This is because the westward flow impinging upon the island's east coast is diverted to the zonal jets, and the westward flow in V_w is decreased by an equivalent amount. In the intermediate region B_{Nw}, the direction of

TABLE 1. Parameters used in the two-and-one-half-layer North Pacific model driven by realistic surface winds.

Parameter	Value
σ_1	23.5
σ_2	26.0
σ_3	27.5
γ_1	0.0240 m s^{-2}
γ_2	0.0143 m s^{-2}
θ_2	35°N
θ_S	19.0°N
θ_N	22.5°N
H_{20}	200 m

the first-layer flow is strongly influenced by the baroclinic structure of the wbc at the northern tip of the island.

South of the southern jet, the ventilated flow returns to the streamlines of the unperturbed gyre while the effects of the northern wbc, the island shadow, and the southern wbc continue to influence the flow to the southwest of the island. If we follow these regions to the southwest, the second-layer pv anomalies persist, but their influence on the first-layer flow decreases as the first layer carries more and more of the Sverdrup transport. A quantitative measure of this trend is discussed below in relation to the effect on the zonal jets of island B.

Perhaps the most interesting consequence of the model is the longitudinal change in the baroclinic structure of the zonal jets, despite the fact that their net transports remain constant, fixed by the net wbc transports at the island's northern and southern tips. We focus on the southern zonal jet because it carries contributions from all of the dynamical regimes produced by the effect of the island and also because it resides within the latitude band of the HLCC. Figure 8 shows a schematic of a vertical section along the centerline of the island A southern jet, with layer velocities drawn to scale relative to each other and layer thicknesses drawn roughly to scale. Near the island, the baroclinic structure of the southern jet is the same as in the wbc at the southern tip of the island. Farther west, the second layer becomes quiescent because of the shadowing effect of the island, and all of the jet transport is carried in the first layer. Farther west still, the baroclinic structure is determined by that of the wbc at the northern tip of the island, and west of this region the structure is determined by the structure of the ventilated flow. In the northern jet, of course, there are only two regions of differing baroclinic structure: that controlled by the northern wbc and that controlled by the ventilated flow.

If the jet were viewed as a continuous zonal flow, the change in baroclinic structure would be a remarkable prediction, but when we realize that the jet is being continuously fed along its northern edge (and depleted along its southern edge) by waters of differing pv characteristics, this becomes an obvious feature. The possibilities for this variation in structure are even richer than might be inferred from Fig. 8. In the ventilated
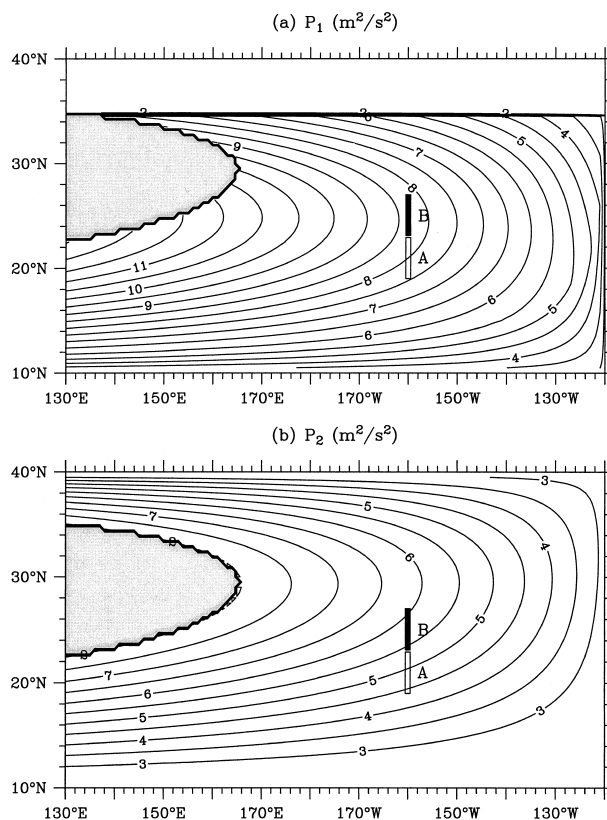

FIG. 6. Pressure distributions in a two-and-one-half-layer ventilated thermocline model driven by the idealized wind stress forcing [(33)]. No island effect is included. Shaded areas indicate the pool region of constant potential vorticity. A and B in the figure denote the two islands whose influences upon the pressure distributions are presented in Figs. 7 and 9, respectively. Island A corresponds to the position of the Hawaiian Islands within the gyre.

part of the jet, H_1 is a constant multiple of H_2 [(5)], so both layers must flow in the same direction, but in the sections of the jet corresponding to regions B_N and B_S, the two active layers could actually flow in opposite directions, depending on conditions in the wbc at the island tips.

b. Island B

To emphasize this point, we investigate the effect of island B, located north of island A, where the first-layer flow impinges upon the island from the northwest, and the second-layer flow still approaches from the northeast. A similar effect could be achieved by rotating island A clockwise relative to the gyre, but the point is that because of the β spiral effect the layer flows are in opposite directions in the northern branch of the wbc. The net transport in this branch is still northward, but the first-layer transport is southward.

Figure 9 shows the layer isobars in the vicinity of island B. Directly west of the island, the picture is qualitatively similar to that for island A. The first-layer flow

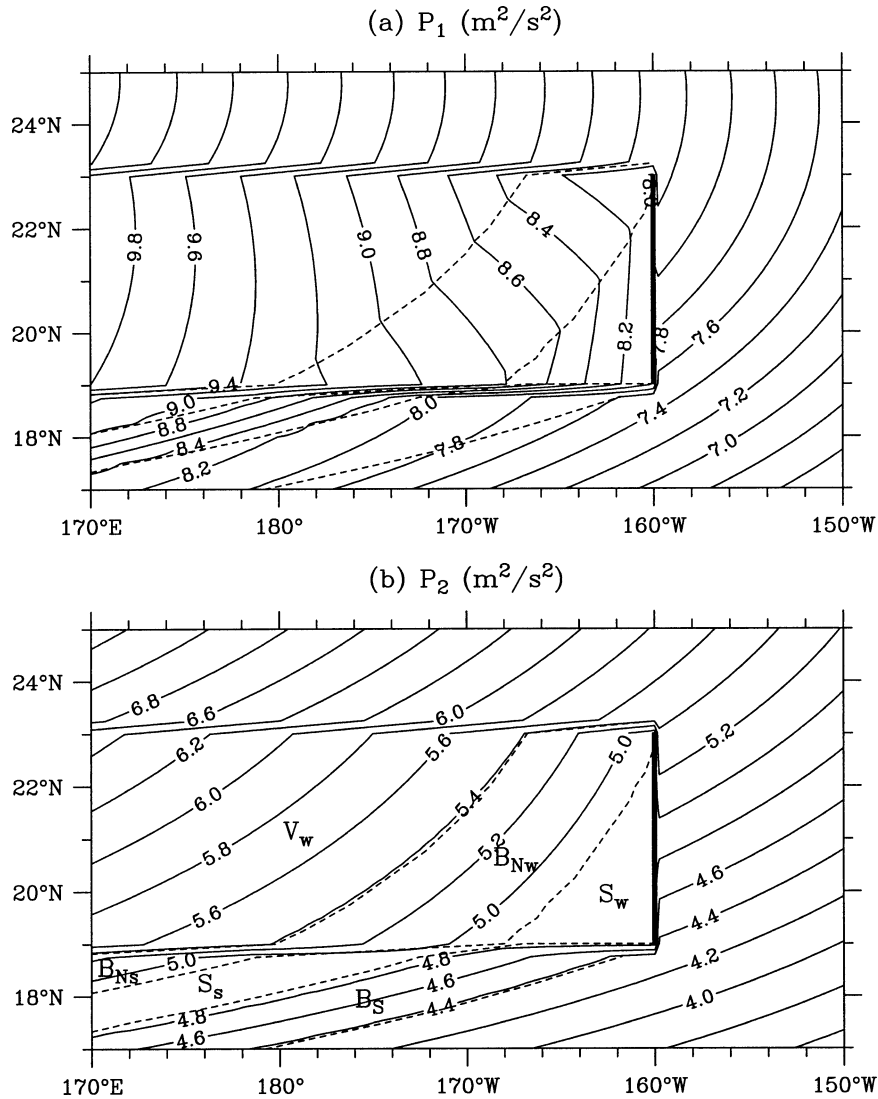## (a) P_1 (m^2/s^2)

(b) P_2 (m^2/s^2)

FIG. 7. Pressure distributions in the neighborhood of Island A, located along 160°W from 19°N to 23°N (A in Fig. 6). Dashed lines denote layer-2 streamlines delineating different dynamic regimes. The broad-scale wind-driven circulation is the same as in Fig. 6.
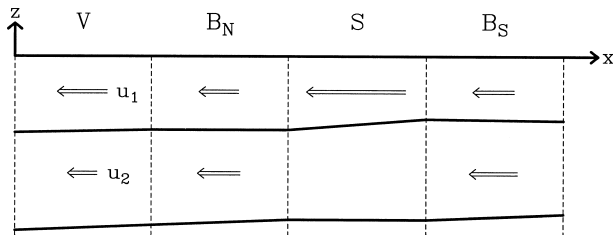

FIG. 8. Vertical section along centerline of the Island A southern zonal jet. Velocity vectors and layer thicknesses are drawn to scale relative to each other. Horizontal dimensions are not drawn to scale: the locations and extents of the individual sections can be seen in Fig. 7.

roughly parallels the island in the shadow zone, and in the ventilated region V_w the isobars are rotated counterclockwise from the islandless gyre isobars because of the blocking of the island. The effect on layer 1 might not be so obvious in this case because the layer-1 flow east of the island is not primarily westward. It is important to remember, however, that the blocking effect diverts the total Sverdrup westward flow east of the island into the zonal jets, thus rotating the total Sverdrup streamlines west of the island. The β spiral effect then determines the angle between the first- and second-layer streamlines. The southward first-layer flow in the northern wbc requires a northward first-layer flow in the northern part of B_{Nw}, resulting in a more pronounced kink in the first-layer streamlines as they cross from V_w to B_{Nw}. It also forces a small circulation zone west of
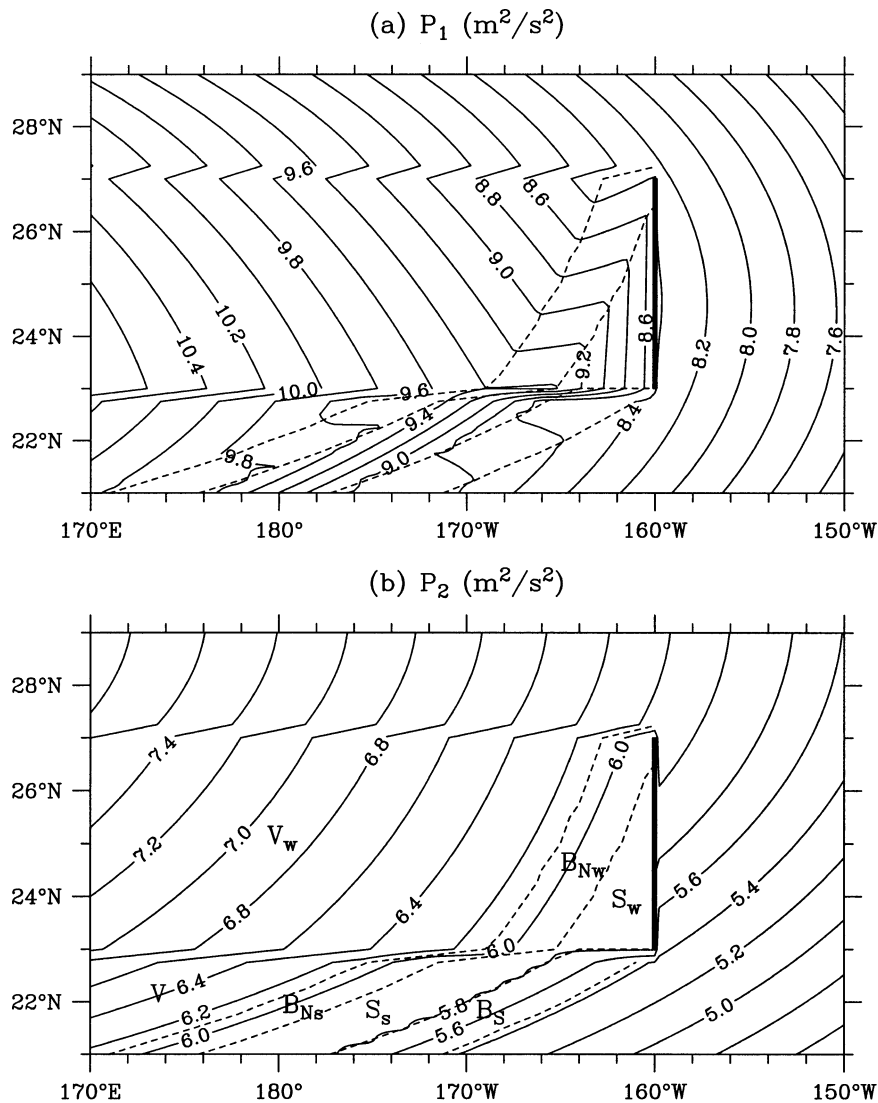
(a) P_1 (m²/s²)

(b) P_2 (m²/s²)

FIG. 9. Pressure distributions in the neighborhood of Island B, located along 160°W from 23°N to 27°N (B in Fig. 6). Dashed lines denote layer-2 streamlines delineating different dynamic regimes.

the northern tip: first-layer water from the north crosses the northern jet flowing westward and then circulates cyclonically to the south, returning to feed the eastward flowing part of the jet near the island.

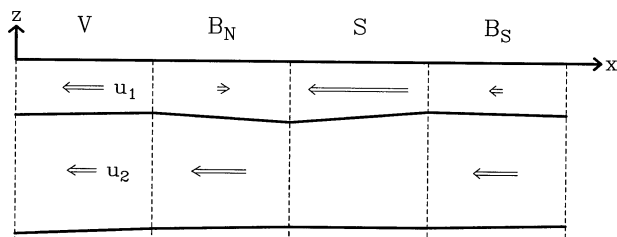Figure 10 shows a schematic of a vertical section

FIG. 10. Same as Fig. 8, but for the case of Island B.

along the centerline of the island-B southern jet, and, as expected, the change in baroclinic structure is much more dramatic than for island A (Fig. 8). Moving westward from the southern tip, the majority of the net transport shifts from the second layer to the first layer, back to the second layer, and finally to a roughly equal partition between layers, with a surface intensification of velocity.

In the northern branch of the island-B wbc, the southward first-layer velocity is almost as great as the northward second-layer velocity, and we might have expected the shear in the B_N section of the southern jet to be greater than that shown in Fig. 10. To understand this, we develop a relationship that is valid between any two points in the gyre connected by a pv-conserving second-layer streamline, but which is particularly enlightening

in this case. We start by defining a baroclinic indicator Π_{12} as the ratio of the first- and second-layer meridional velocities:

$$\Pi_{12} \equiv \frac{v_1}{v_2} = \frac{\partial \pi_1/\partial x}{\partial \pi_2/\partial x} = 1 + \Gamma_{12}\frac{\partial H_1/\partial x}{\partial H_2/\partial x}, \quad (34)$$

where π_i is the dynamic pressure in layer i, $\Pi_{12} = 1$ corresponds to equal meridional velocities in the same direction, and $\Pi_{12} = -1$ corresponds to equal but opposite meridional velocities. We next notice that pv conservation across a meridionally thin jet results in the layer-1 and layer-2 streamlines crossing the jet coincidentally, and the zonal gradients of H_1 and H_2 along the northern edge of a jet are mapped by the streamlines onto meridional gradients within the jet such that the ratio $\Delta H_1/\Delta H_2$ remains constant through the mapping. Consequently, Π_{12} gives the layer velocity ratio within the zonal jets as well as at the wbc outflows. For region B_N,

$$\Pi_{12}(\theta) = 1 + \Gamma_{12}\left(1 - \frac{f}{f_N}A_N\right), \quad (35)$$

where A_N is defined in (16), and in the ventilated region V

$$\Pi_{12}(\theta) = 1 + \Gamma_{12}\left(1 - \frac{f}{f_2}\right). \quad (36)$$

More generally, it is easy to show that if Π_{12} is known at some latitude, say, θ_N, then at another latitude on the same pv-conserving streamline,

$$\Pi_{12}(\theta) = \frac{f}{f_N}\Pi_{12}(\theta_N) + \left(1 - \frac{f}{f_N}\right)(1 + \Gamma_{12}). \quad (37)$$

It is clear that as f approaches 0, Π_{12} tends monotonically toward $(1 + \Gamma_{12}) > 1$, so that as a pv-conserving streamline is followed equatorward, the meridional flow and the flow in any zonal jet that is crossed tend toward a unidirectional, surface intensified flow. In the case of island B, the velocity ratio changes from $\Pi_{12} = -0.6$ at the outflow of the northern boundary current to $\Pi_{12} = -0.15$ where B_N crosses the southern jet. For island A, the velocity ratio changes from $\Pi_{12} = 0.6$ at the outflow of the northern wbc to $\Pi_{12} = 0.9$ where B_N crosses the southern jet.

Equation (37) also shows that the difference between values of Π_{12} on two different streamlines decreases monotonically as one moves equatorward. Specifically, we quantify the change in baroclinic structure from the B_N part of the jet to the ventilated (V) part of the jet as the change in the value of Π_{12}:

$$\Delta\Pi_{12}(\theta) = \Pi_{12V}(\theta) - \Pi_{12B_N}(\theta), \quad (38)$$

and (37) shows that

$$\Delta\Pi_{12}(\theta_S) = \left(\frac{f_S}{f_N}\right)\Delta\Pi_{12}(\theta_N). \quad (39)$$

For island A, this indicator changes from $\Delta\Pi_{12} = 1.0$ in the northern jet to $\Delta\Pi_{12} = 0.8$ in the southern jet, and for island B it changes from $\Delta\Pi_{12} = 2.0$ in the northern jet to $\Delta\Pi_{12} = 1.7$ in the southern jet.

The above analysis was for an infinitesimally thin zonal jet, and we briefly look at the effect of relaxing the width restriction by looking at the jet in the ventilated region. In a jet of finite width, the layer isobars do not cross the jet coincidentally, and the β effect must be considered in calculating the ratio of zonal velocities. We find that

$$\frac{u_1}{u_2} = \Pi_{12}[1 - \epsilon(x, y)], \quad (40)$$

where

$$\epsilon(x, y) = \frac{\Gamma_{12}\beta}{f_2 + \Gamma_{12}(f_2 - f)}\frac{H_2}{\partial H_2/\partial y}. \quad (41)$$

For a given pressure jump across the jet, clearly ϵ approaches 0 as Δy approaches 0. For a realistic jet width on the order of 100 km and the model values of H_2, ΔH_2, and f in the southern jet not too far west of the island, $\epsilon = O(0.1)$, and Π_{12} is a good proxy for u_1/u_2. In the sections B_N and B_S the expression for ϵ is more complicated, but the results are qualitatively similar. The important thing to note, however, is that u_1/u_2 is now a function of longitude. For a given jet transport, $\partial H_2/\partial y$ decreases as H_2 increases, so that farther west where the gyre deepens, we would expect u_1/u_2 to depend sensitively on longitude. In section 4 we will see that this is indeed the case.

c. Conceptual summary

The effect of the island on the two-and-one-half-layer interior flow is most easily conceptualized as the creation of two overlapping wakes: a transport wake that alters the barotropic transport patterns directly west of the island, and a pv wake that alters the baroclinic nature of the circulation downstream from the island, in the sense of second-layer streamlines. The transport wake is characterized by a diversion of the normal component of the interior flow incident upon the east coast of the island into two zonal jets at the northern and southern extremes of the wake. In the event that the wind stress circulation around the island is nonnegligible, the zonal jets carry an additional transport forced by the anomalous wind along the west coast of the island. This additional transport is equal in the two jets but is oppositely directed. Between the jets, the effect of the transport wake is to superimpose an anomalous eastward net transport, which for a thin island is equal to the transport blocked by the island within the same zonal band. This anomalous eastward transport is independent of longitude, and over the full meridional span of the island it is equal in magnitude to the westward transport carried by the jets. In section 4 we will be concerned with how inclusion of the island–interior flow interaction alters

model estimates of the HLCC transport, and the above points make it clear that this effect depends sensitively on the location of the HLCC boundaries within the transport wake. The anomalous eastward transport will be divided between the layers, and how it is divided depends on the pv characteristics of the region. We will see in section 4 that the partitioning between layers is independent of longitude within the ventilated region, but this is not generally true of the other regions.

The pv wake is characterized by a loss of the ventilated pv signature in the second layer, and it extends equatorward and westward from the island, sandwiched between two ventilated second-layer streamlines. It contains three bands of distinct pv characteristics: two side-bands in which the second-layer pv is determined at the northern and southern wbc outflows and a central shadow zone in which the second layer is quiescent. The side band widths are proportional to the net wbc transports at the outflows and are inversely proportional to the strength of the Sverdrup forcing at the outflows.

In the shadow zone, the first-layer streamlines obviously are parallel to the geostrophic Sverdrup transport streamlines. The layer-2 streamlines that would otherwise have been found within the area occupied by the shadow zone are squeezed into the pv wake side bands fed by the wbc outflows, thus increasing the second-layer velocity in these bands while maintaining the unperturbed directionality. The velocity anomalies in the side bands are on the order of 100%; the second-layer thickness anomalies are typically of the order of 10%. To lowest order, then, the effect on first-layer flow in the side bands can be estimated by equating relative velocity and transport anomalies in the second layer. The increased transport in the second-layer demands an equal and opposite transport in the first layer, causing the first-layer streamlines to be rotated cyclonically in Figs. 7 and 9. As one follows the pv wake equatorward, the second-layer pv anomalies persist, but the anomaly in the first-layer streamlines decreases as the first-layer thickens and carries proportionally more of the Sverdrup transport.

Directly west of the island the transport wake and the pv wake overlap, and the effects discussed above are superimposed. Perhaps the most interesting consequence is the creation of a southern zonal jet with a constant net transport but with a baroclinic structure that changes, possibly dramatically, through four distinct sections. From the island and proceeding westward, the baroclinic structure is controlled by the outflow of the southern wbc, the shadow zone, the outflow of the northern wbc, and the ventilated pv characteristics. For model parameters representative of the North Pacific and the Hawaiian Islands, the layer flow in the ventilated part of the jet nearest the island is unidirectional and the velocity ratio is nearly independent of longitude. As the gyre deepens to the west, however, the ventilated jet baroclinicity changes gradually, and the velocities can

become oppositely directed before reaching the western boundary.

In a model with more than two active layers, each subsurface layer will have its own pv wake, creating a pv wake "fan" in which the wake directions rotate anticyclonically with depth. This pv wake fan is analogous to, although simpler than, the fan of characteristics described by Huang and Pedlosky (2000) in connection with extratropical buoyancy forcing of a multilayer model. In their case, a pv anomaly introduced at the subduction zone of a deep layer propagates equatorward, creating a cascade of pv anomalies in shallower layers such that the number of new pv anomaly cones (wakes) created doubles at each successive subduction zone. In our case, the island resides equatorward of all subduction zones, it creates pv anomalies in all layers concurrently, and each layer gets a single pv wake (cone). The downstream broadening of the pv anomaly influence from the β spiral effect would be similar in the two cases. For islands located progressively equatorward, the transport and pv wakes become more colinear (cf. Figs. 7 and 9). For an island at the equatorward limit of the subtropical gyre, the wakes would become coincident, the zonal jets would become true extensions of the wbc with no change in baroclinic structure, and the shadow zone would occupy the entire region between the zonal jets.

4. Application to the North Pacific Ocean

In this section, we apply the theory of the previous two sections to a more realistic representation of the North Pacific Ocean. For the surface wind stress data, we adopt the climatology from the European Centre for Medium-Range Weather Forecasts reanalysis. This dataset is one of the wind products used in the numerical modeling study of the HLCC by Xie et al. (2001). Figure 11 shows the distribution of the Ekman pumping velocity w_E, calculated from the ECMWF wind stress dataset. The broad-scale pattern is similar to that used in previous ventilated thermocline studies of the North Pacific (Talley 1985; Huang and Russell 1994): the zero Ekman pumping line tilts southwest–northeast from south of Japan at 30°N in the west to Vancouver Island at 50°N in the east, and w_E is on the order of -1×10^{-6} m s^{-1} over the broad region of the subtropical North Pacific Ocean. A noticeable feature that was missing from older surface wind stress climatologies, however, is the dipole Ekman pumping velocity structure present southwest of the Hawaiian Islands. As noted by Xie et al. (2001), this dipole w_E structure is due to the high elevation of the mountains Haleakala, Mauna Loa, and Mauna Kea on the two southern islands of the Hawaiian island chain. In Fig. 11, the maximum $\pm w_E$ values associated with the island orography are 4.4×10^{-6} and -8.0×10^{-6} m s^{-1}, respectively.

In Fig. 12 we plot the pressure distributions for a two-and-one-half-layer North Pacific model using LPS
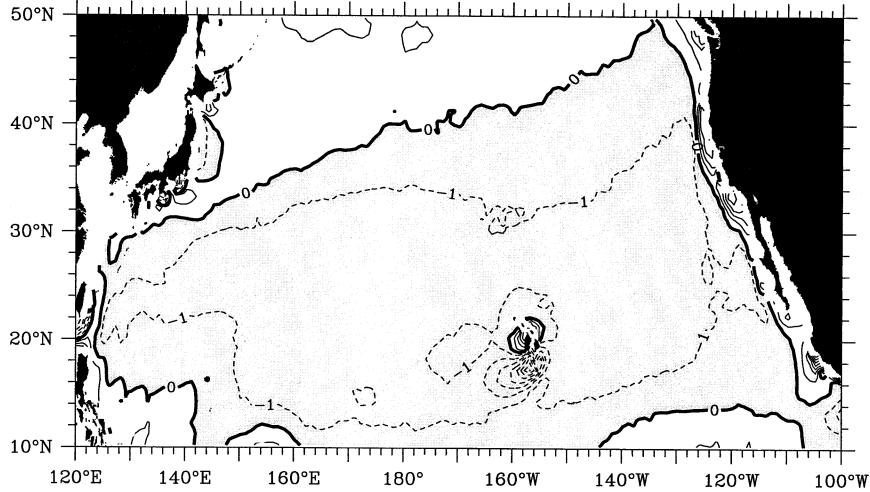
FIG. 11. Ekman pumping velocity w_e calculated from the climatological surface wind stress data of ECMWF (1982–98). Contour intervals are 1×10^{-6} m s^{-1}. Shaded areas indicate $w_e < 0$. Notice the dipole structure around the Hawaiin Islands where the maximum $\pm w_e$ values are 4.4×10^{-6} and -8.0×10^{-6} m s^{-1}, respectively.
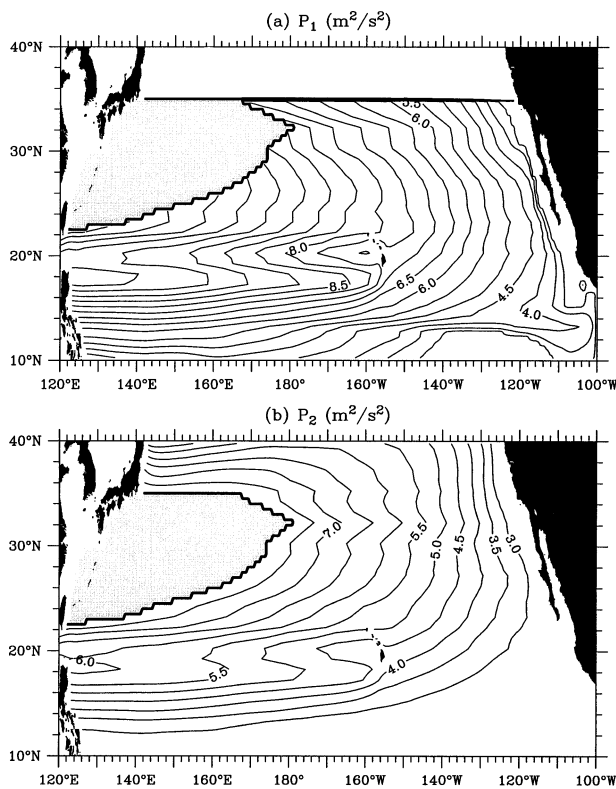

FIG. 12. Pressure distributions in (a) the surface layer and (b) the second layer from a two-and-one-half-layer North Pacific model driven by the climatological ECMWF wind stress data. Blocking of the interior transport by the Hawaiian Islands is not included in this figure. Shaded areas indicate the pool region of constant potential vorticity. Note that the pressure values are related to the layer thickness values by $P_1 = \gamma_1 H_1 + \gamma_2 H_2$ and $P_2 = \gamma_2 H_2$.

dynamics and ECMWF wind forcing but intentionally ignoring the blocking effect of the Hawaiian Islands on the interior flow. Parameter values pertinent to the model are listed in Table 1 and the predicted island wbc transports are shown in Table 2. As partial support for the appropriateness of the wind product, we note that the predicted net wbc transport at 22.5°N of +3.56 Sv (Sv $\equiv 10^6$ m^3 s^{-1}) agrees favorably with the observed wbc (i.e., the North Hawaiian Ridge Current) transport estimate of 3.24 Sv based on multiyear ADCP measurements north of Oahu Island (Firing 1996; Qiu et al. 1997). Because the P_1 and P_2 contours coincide with the streamlines of the first- and second-layer geostrophic flows, it is clear from Fig. 12 that an eastward flow exists in both the first and second layers in the zonal band between 18° and 20°N, west of the Hawaiian Islands. The location of this band of eastward flow corresponds well with that of the observed HLCC (Fig. 1). Dynamically, this eastward flow is due to the presence of the dipole w_E forcing southwest of the Hawaiian Islands, as shown in Fig. 11. Although this is obviously an effect of the island on the atmosphere, in what follows we use the term "island effect" exclusively to

TABLE 2. Western boundary current transports (Sv) at the southern and northern tips of the Hawaiian Islands from the model forced by the ECMWF wind stress data. Here, T_{Wj} is the wbc transport in the jth layer (northward positive) and $T_{W1} + T_{W2}$.

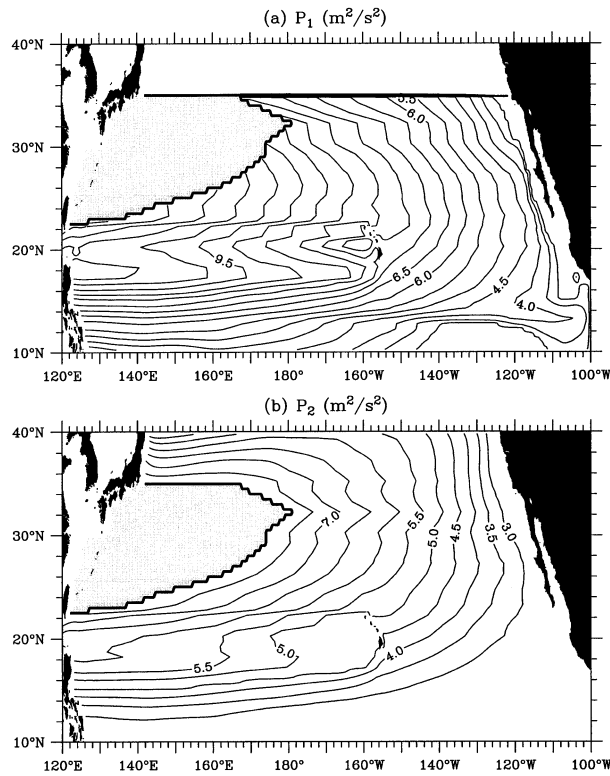| Transport	Value (Sv)
$T_{W1}\ (\theta_S)$	−0.23
$T_{W2}\ (\theta_S)$	−1.17
$T_{Wnet}\ (\theta_S)$	−1.40
$T_{W1}\ (\theta_N)$	1.37
$T_{W2}\ (\theta_N)$	2.19
$T_{Wnet}\ (\theta_N)$	3.56

FIG. 13. Same as Fig. 12 except that the blocking by the Hawaiian Islands is taken into account in the ventilated thermocline model. Detailed formulations are presented in section 2.
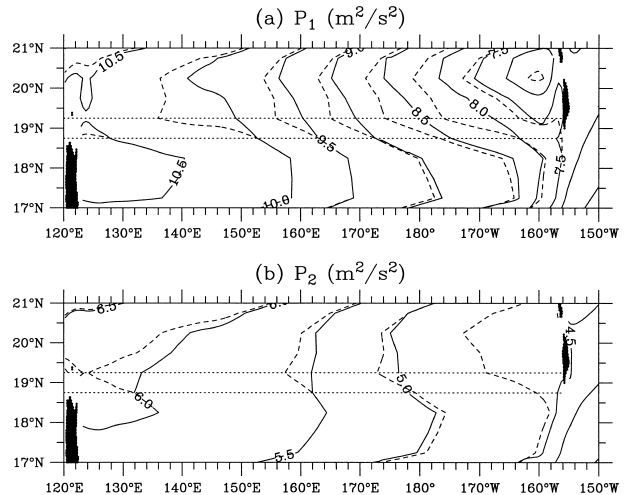

FIG. 14. Comparisons between the modeled (a) first-layer and (b) second-layer pressure fields west of the Hawaiian Islands, with and without the island effect. Dashed lines represent the isobars without the inclusion of the island effect, and solid lines are with the island effect included. The effect of the southern zonal jet is shown distributed over the ½° band delineated by the dotted lines, corresponding to the model resolution.

mean the effect of the island on the oceanic interior flow.

For comparison, we plot in Fig. 13 the pressure fields derived after taking into account the presence of the Hawaiian Islands using the methodology of section 2. The island effect is confined to the region west of the Hawaiian Islands between the latitude θ_N and the lower-layer pressure contour Φ_S (the southern boundary of the pv wake). With the ECMWF wind forcing, Φ_S extends from 19°N at the southern tip of the Hawaiian Islands to 15°N near the western boundary. More important, the location of the southern zonal jet discussed in section 2 falls within the latitude band of the eastward current seen in Fig. 12. As with the idealized winds of section 2, the ECMWF winds produce a southward wbc at the southern tip of the island, so the corresponding westward southern zonal jet of our model would be in direct opposition to the eastward current forced by the w_E dipole.

In Figs. 14a,b we enlarge the region west of Hawaii and superimpose the isobars of Figs. 12 and 13. The w_E-dipole-only isobars are dashed; the dipole-plus-island-effect isobars are solid. The numerical grid used to generate the figures has a 0.5° resolution, and because we do not address boundary current or jet structure, the effect of the zonal jets is distributed across the 0.5° bands centered on the latitudes of the northern and

southern tips of the islands (see dotted lines in figures). Despite the lack of a westward jet in the southern band, we will continue to refer to this band as the southern jet to maintain continuity with the terminology of our model. The most obvious effect visible in Fig. 14 is that, as expected, including the island effect decreases the eastward transport in the region of the southern jet. A more subtle but equally important point is that the eastward transport is increased slightly in the region north of the southern jet. This is because of the transport wake effect discussed at the end of section 3. The net reduction in the eastward transport of the HLCC caused by the island effect is clearly dependent on the latitude of the northern edge of the HLCC.

For a look at the influence of the island effect on the baroclinic structure of the HLCC and a more quantitative measure of the transport reduction, we plot in Figs. 15b,c the longitude-dependent zonal transport values in the first and second layers within the 18.25°–20.25°N band. The dashed lines are the results without the island effect, and the solid lines have the island effect included. Notice that the net (sum of first and second layer) eastward transport reduction caused by the island effect is independent of longitude, as discussed in section 3. The net change is −0.88 Sv, with the 18.75°–19.25° band (southern jet) contributing −1.40 Sv and the 19.25°–20.25° band contributing +0.52 Sv. The southern jet contribution is equal to the net wbc transport at the southern tip of the Hawaiian Islands [$T_{W\text{net}}(\theta_S)$ in Table 2]. Properly considering the island effect results in a reduction of the predicted HLCC transport of about 20% and a reduction of the predicted transport within the 18.25°–19.25°N band of about 40%.
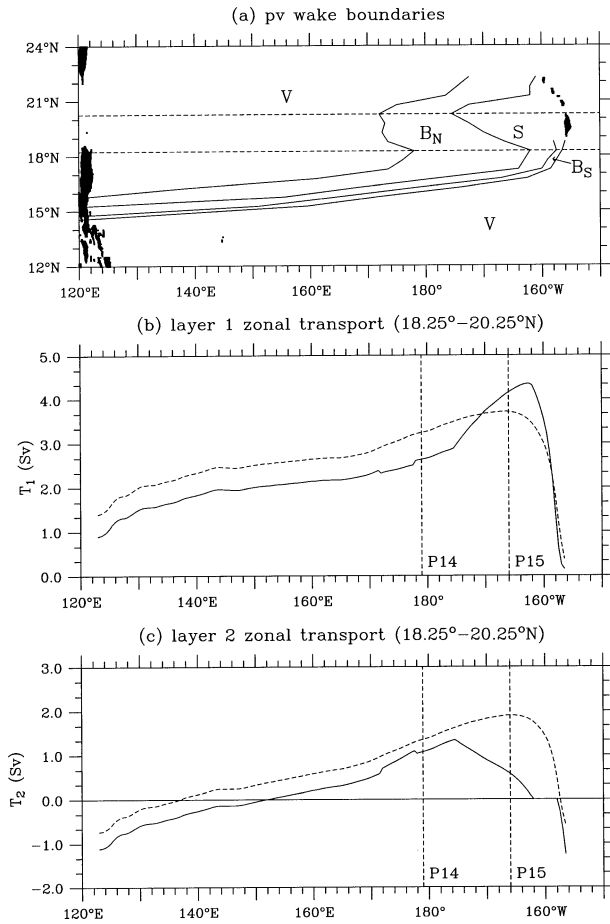
FIG. 15. (a) Boundaries delineating the subregions of the pv wake and the zonal band of eastward flow for which transports are shown in (b) and (c). (b) Upper-layer zonal transport in the band of 18.25°–20.25°N. Dashed line shows the value in the case in which the presence of the Hawaiian Islands is ignored, and solid line shows the value when the Hawaiian Islands are included. (c) Same as (b), but for the lower-layer zonal transport. Simulations are for the ECMWF wind-forcing case.

How the net transport reduction is distributed between the two layers depends, of course, on the location within the pv wake. In Fig. 15a we show the boundaries of the pv wake and of the subsections B_N, S, and B_S. Also shown are the boundaries of the zonal strip representing the HLCC, within which the transports of Figs. 15b and 15c are calculated. The crossing of the HLCC by the pv wake creates a zonally varying baroclinic structure (visible in Figs. 15b,c) that is similar to that for island A in section 3 (Fig. 8). In the islandless case (dashed lines), the layer transport ratio changes only very gradually in response to the westward deepening of the gyre as discussed at the end of section 3 [(40)]. This effect is also visible when the island is included (solid lines), but a much more dramatic change in the transport ratio is seen where the current passes through the shadow zone of the pv wake. The difference in structure between the regions B_N and V is subtle, just as it was for island

A in section 3 (Fig. 8). The changes could be more dramatic for an island oriented differently with respect to the gyre, as with island B of section 3, but for the Hawaiian Islands the main difference in baroclinic structure is between the shadow zone S and the rest of the current (in B_S the flow is predominantly southward, with weak zonal currents that are oppositely directed because of the β spiral effect). In section 1, we showed ADCP sections from the WOCE transects P14 and P15 (Fig. 2) and noted that the eastward flow in the 18°–20°N band of P15 is significantly surface intensified as compared with the flow at the same latitude of P14. The locations of these two transects are shown in Figs. 15b,c. We again emphasize that this is a region of relatively high eddy activity, so that snapshots in time are far from conclusive. However, it is interesting to note that P15 falls close to the model's predicted shadow zone, where the lower layer would be expected to be quiescent. The current in P15 is confined primarily to the upper 150 m, which corresponds closely with the model layer-1 thickness at this location.

Two other points are worth noting with regard to Fig. 15. One is that, although the plots of centerline velocities in Figs. 8 and 10 show abrupt changes in structure, the transport integrated over the width of the current changes gradually because of the overlap of the distinct pv regimes within a finite length of the current (Fig. 15a). The other is that although the layer transport ratio within the ventilated zone V is longitude dependent [(40)], the ratio of the layer transport reductions (differences between solid and dashed lines) is not. Because conditions in the ventilated region V south of θ_S are not changed by inclusion of the island effect, the second-layer transport change within a zonal band between θ_- (south of the zonal jet) and θ_+ (north of the zonal jet) is

$$T_2 - \tilde{T}_2$$

$$= -\frac{\gamma_2}{2f_2}[H_2^2(\phi, \theta_+) - \tilde{H}_2^2(\phi, \theta_+)]$$

$$= -\frac{\gamma_2}{2f_2}\left\{\frac{H_{2I}^2 + \Gamma_{12}H_{1i}^2(\theta_+)}{1 + \Gamma_{12}(1 - f_+/f_2)^2} - \tilde{H}_2^2[\phi_{I\omega}(\theta_+), \theta_+]\right\},$$

where $\tilde{\ }$ denotes values calculated without the island, and ϕ_{Iw} is the longitude of the west coast of the island. The layer-2 transport reduction in the ventilated zone is clearly longitude independent. Because the net transport reduction is also longitude independent, it follows that the same holds for the layer-1 reduction and for the ratio of the layer transport reductions in the ventilated zone.

5. Effect of pv diffusion within zonal jets

Throughout the above model development, we have assumed that the second-layer pv (q_2) is conserved along streamlines crossing the zonal jets at the latitudes of the northern and southern tips of the island. If dif-

fusion is significant within a jet, q_2 will be modified according to

$$\frac{D}{Dt}q_2 = \boldsymbol{\nabla} \cdot (A_h \boldsymbol{\nabla} q_2) + \frac{\partial}{\partial z}\left(A_z \frac{\partial}{\partial z}q_2\right), \quad (42)$$

where D/Dt is the material derivative following a second-layer parcel across the jet, and A_h and A_z are the horizontal and vertical eddy viscosity coefficients. The net change in q_2 is largely determined by the thickness fluxes. The change caused by the diffusion of relative vorticity is small by comparison, because ζ and its derivatives have opposite signs on the two sides of the jet and the diffusive effects tend to cancel out when integrated across the jet.

For the horizontal dissipation, the net change in q_2 is dominated by the cross-stream diffusion, which can be approximated by

$$\Delta q_2 \approx A_h \Delta t \frac{L^2}{W^2}\overline{\frac{\partial^2 q_2}{\partial x^2}},$$

where Δt is the time required for the particle to cross the jet, L is the zonal extent of the jet crossing, $W \ll L$ is the jet width, and the overbar denotes the average along the particle trajectory. Assuming that the relative change in w_E is small over the length of the crossing and using the pv conserving model to evaluate the parameters, we have

$$\overline{\frac{\partial^2 q_2}{\partial x^2}} \approx \frac{3f_2}{H_2^5}\frac{f^4(-w_E)^2}{\beta^2\gamma_2^2[1 + \Gamma_{12}(1 - f/f_2)^2]^2},$$

where L is constrained by (1) and (3), and Δt is constrained by W and the mean second-layer meridional velocity, so that near the northern tip of the island,

$$L = \frac{\beta\gamma_2}{2f_N^2(-w_E)}[H_{2WN}^2 + \Gamma_{12}H_{1WN}^2 - (H_{2I}^2 + \Gamma_{12}H_{1I}^2)],$$

and

$$\Delta t = \left|\frac{W}{v_2}\right| = \frac{W\beta H_{2WN}}{f_N(-w_E)}\left[1 + \Gamma_{12}\left(1 - \frac{f_N}{f_2}\right)^2\right].$$

Parameter values appropriate for the Hawaiian Islands and ECMWF wind forcing (see section 4) are $\beta = 2.1 \times 10^{-11}$ m^{-1} s^{-1}, $f_N = 5.58 \times 10^{-5}$ s^{-1}, $f_S = 4.75 \times 10^{-5}$ s^{-1}, $w_E = -1.2 \times 10^{-6}$ m s^{-1}, $H_{2WN} = 360$ m, $H_{1WN} = 122$ m, $H_{2WS} = 301$ m, $H_{1WS} = 128$ m, $H_{2I} = 321$ m, and $H_{1I} = 119$ m. Using $A_h = 1000$ m^2 s^{-1}, based on Stammer[2] (1998; his Fig. 5a), and a jet width comparable to the observed width of the North Hawaiian Ridge Current, $W = 10^5$ m, the relative change in q_2 from horizontal diffusion during the crossing of the

---

[2] Stammer estimated A_h values based on TOPEX/Poseidon measurements of sea surface height variability. These measurements are largely associated with thermocline variability and thus provide a good measure of eddy diffusivity within the thermocline.

---

northern jet is 3.3%. The strong anomalous Ekman pumping overpowers the southern jet effect in our realistic scenario, but in the absence of the anomalous w_E, a similar analysis gives a relative change in q_2 across the southern jet of less than 1%.

For the vertical eddy diffusion, an estimate of the pv difference between layers 1 and 2 leads to

$$\frac{\Delta q_2}{q_2} \approx A_z\Delta t \frac{2(H_2 - 2H_1)}{H_1 H_2(H_2 - H_1)}$$

$$\approx \frac{2A_z\beta W(H_2 - 2H_1)}{fH_1(H_2 - H_1)(-w_E)}\left[1 + \Gamma_{12}\left(1 - \frac{f}{f_2}\right)^2\right]. \quad (43)$$

Using the upper bound for the vertical eddy viscosity coefficient, $A_z = 10^{-4}$ m^2 s^{-1}, we calculate $\Delta q_2/q_2 = 3.0\%$ (3.2%) for the northern (southern) jet near the island. Because of the conservative choice of A_z, this estimate is most likely high.

The combined effect of horizontal and vertical diffusion is thus expected to produce a relative change in second-layer pv of less than 6% (4%) during the crossing of the northern (southern) jet near the longitude of the Hawaiian Islands. Farther to the west, the gyre deepens and the jets widen, and both of these effects will reduce the diffusion within the jets, thus rendering the effect on second-layer pv even smaller. Consequently, the above numbers are not additive for a single streamline. The first streamline to cross both jets, Φ_N, would see a relative change in q_2 across the southern jet of less than 2%. The smallness of the jet-crossing effect justifies the pv-conserving assumption adopted at the outset of our study.

6. Conclusions

This study is motivated by recent observational and modeling studies that described the existence of the Hawaiian Lee Countercurrent and its forcing by the island-perturbed, anomalous surface winds. Our objective has been to understand how the picture of an eastward flow forced strictly by wind anomalies west of the Hawaiian Islands is altered by considering the interaction of the islands with the interior flow forced by winds to the east. In pursuit of this goal, we extend the two-and-one-half-layer ventilated thermocline model to include an island in the ventilated midgyre, at a location where the Sverdrup interior flow impinges upon the island from the east. The model gives the following picture of the effect of the island on the wind-driven, ventilated circulation.

The island creates two wakes, which we call a transport wake and a pv wake. The transport wake extends west of the island and is characterized by an alteration of the zonal component of the barotropic transport. The normal transport impinging upon the east coast of the island is redirected to westward flowing zonal jets that bound the transport wake on the north and south. Be-

tween the jets, the transport wake creates an anomalous eastward transport that is superimposed on the islandless solution in compensation for the transport blocked by the island. The barotropic transport of each jet, and of the anomalous eastward flow between the jets, is independent of longitude.

The pv wake is characterized by a loss of the ventilated pv signature in the second layer. It extends equatorward and westward from the island, sandwiched between two ventilated second-layer streamlines. It contains three bands of distinct pv characteristics: two in which the second-layer pv is determined at the northern and southern wbc outflows, and a central shadow zone in which the second layer is quiescent. The second-layer pv anomalies persist within the wake, but the consequent anomalies in the first layer flow decrease to the south. The crossing of the two wakes in the immediate lee of the island creates a southern zonal jet with a constant net transport but with a baroclinic structure that changes, possibly dramatically, through four distinct sections.

Using the ECMWF climatological wind stress data, we show that, although the primary forcing for the eastward-flowing HLCC may be the dipolar Ekman pumping velocity anomalies generated by the island orography, inclusion of the interaction between the Hawaiian Islands and the wind-driven subtropical circulation significantly alters both the strength and the baroclinic structure of the modeled HLCC. Specifically, we find that the pressure gradient corresponding to the transport wake's southern jet acts to weaken the southern part of the eastward-flowing HLCC while the anomalous eastward transport in the center band of the transport wake strengthens the northern part of the HLCC. Under the ECMWF wind forcing, the net eastward transport of the modeled HLCC is decreased by about 20% when the island effect is properly included, and the transport in the southern half of the modeled HLCC is decreased by about 40%. The pv wake concept predicts a change from a surface-intensified HLCC near the islands to a more barotropic current further west. Available ADCP measurements, while not conclusive, are consistent with this picture.

Aside from the estimate of pv diffusion during the crossing of the zonal jets, the consideration of diffusive effects has been beyond the scope of this work. We expect that the boundaries between dynamical regions will in fact be smoothed, but this should have minimal impact on the characteristics of regions with large spatial scales. In particular, we have shown that the primary impact on the baroclinic circulation west of the Hawaiian Islands involves the island shadow zone, and the shadow zone produced by realistic winds and coastal geometry (Fig. 15a) has a zonal scale on the order of 1000 km. Consequently, we expect the predicted baroclinic structure of the HLCC to be qualitatively robust.

APPENDIX A

Consequence of Dynamic Similarity within Western Boundary Current Layers

When the flow regimes within the separate wbc layers are similar enough that they can be considered as governed by the same dynamics, the current velocity in layer j can be expressed as

$$v_j = a_j g(x), \qquad 0 \leq x \leq \delta, \tag{A1}$$

where a_j is a layer-dependent constant (positive or negative), $g(x)$ is a layer-independent structure function, and δ is a layer-independent boundary current width. Working from the bottom layer up, (A1) yields

$$\partial H_i / \partial x = b_j g(x),$$

with b_j being another constant. Consequently,

$$H_j(x) = H_{jI} + b_j \int_{x_I}^{x} dx' \, g(x')$$

$$= H_{jI} + (H_{jw} - H_{jI}) G(x), \tag{A2}$$

where

$$G(x) = \frac{\int_{x_I}^{x} dx' \, g(x')}{\int_{x_I}^{\delta} dx' \, g(x')}$$

has been normalized so that $G(\delta) = 1$. It is now clear that

$$\frac{H_1(x) - H_{1I}}{H_{1w} - H_{1I}} = \frac{H_2(x) - H_{2I}}{H_{2w} - H_{2I}}, \tag{A3}$$

H_1 is a linear function of H_2, and (12) follows.

APPENDIX B

Transition from Western Boundary Current to Sverdrup Regime

If we impose the layer self-similarity condition on both the wbc at $I_N - O_{Nn}$ and the Sverdrup flow at $I_N - O_{Ns}$ (see Fig. 4), we have

$$H_j = H_{jI} + (H_{jWN} - H_{jI})G(x),$$

$$0 \leq x \leq \delta, \quad \text{at } I_N - O_{Nn}, \quad \text{and} \quad \text{(B1)}$$

$$\hat{H}_j = H_{jI} + (H_{jWN} - H_{jI})\hat{G}(\hat{x}),$$

$$0 \leq \hat{x} \leq \hat{\delta}, \quad \text{at } I_N - O_{Ns}, \quad \text{(B2)}$$

where j is a layer index, and the hatted and unhatted variables have the same dimensions but refer to the different transects; x and $\hat{x}$ are the along-transect coordinates originating at I_N and increasing northward in the case of x and westward in the case of $\hat{x}$. In this formulation, geostrophic streamlines clearly map x onto $\hat{x}$ such that $\hat{G}(\hat{x}) = G(x)$. The structure functions G and $\hat{G}$, however, can be very different from each other. To prevent the streamlines from crossing during the mapping, G and $\hat{G}$ need only have the same number of extrema within the given interval, with the same values at the extrema. In an idealized model, a reasonable specification might be that they both be monotonic. Aside from this, G can be chosen to satisfy the wbc dynamics, and $\hat{G}$ is chosen to satisfy the Sverdrup dynamics at $I_N - O_{Ns}$. By definition, the total mass transport is the same across the two transects, but the requirement that H_1 and H_2 maintain the self-similar structure throughout the transition region guarantees that it is also conserved locally; that is, the geostrophic streamlines are true mass transport streamlines. At $I_N - O_{Nn}$, the layer-2 transport between x and $x + dx$ is

$$T_2 = h_2(x)\frac{\gamma_2}{f_n}(H_{2WN} - H_{2I})\frac{dG}{dx}dx. \quad \text{(B3)}$$

At $I_N - O_{Ns}$ the layer-2 transport between $\hat{x}(x)$ and $\hat{x}(x + dx)$ is

$$\hat{T}_2 = \hat{h}_2(\hat{x})\frac{\gamma_2}{f_n}(H_{2WN} - H_{2I})\frac{d\hat{G}}{d\hat{x}}[\hat{x}(x + dx) - \hat{x}(x)]$$

$$= h_2(x)\frac{\gamma_2}{f_n}(H_{2WN} - H_{2I})\frac{d\hat{G}}{d\hat{x}}\frac{d\hat{x}}{dx}dx = T_2,$$

because $\hat{G}(\hat{x}) = G(x)$ implies both

$$\hat{h}_2(\hat{x}) = h_2(x) \quad \text{and} \quad \frac{d\hat{G}}{d\hat{x}}\frac{d\hat{x}}{dx} = \frac{dG}{dx}.$$

REFERENCES

Aoki, Y., T. Suga, and K. Hanawa, 2002: Subsurface subtropical fronts of the North Pacific as inherent boundaries in the ventilated thermocline. *J. Phys. Oceanogr.,* **32,** 2299–2311.

De Szoeke, R. A., 1987: On the wind-driven circulation of the South Pacific Ocean. *J. Phys. Oceanogr.,* **17,** 613–630.

Firing, E., 1996: Currents observed north of Oahu during the first five years of HOT. *Deep-Sea Res.,* **43,** 281–303.

Flament, P., R. Lumpkin, J. Tournadre, and L. Armi, 2001: Vortex paring in an unstable anticyclonic shear flow: discrete subharmonics of one pendulum day. *J. Fluid Mech.,* **440,** 401–409.

Godfrey, J. S., 1989: A Sverdrup model of the depth-integrated flow for the world ocean allowing for island circulations. *Geophys. Astrophys. Fluid Dyn.,* **45,** 89–112.

Huang, R. X., and S. Russell, 1994: Ventilation of the subtropical North Pacific. *J. Phys. Oceanogr.,* **24,** 2589–2605.

——, and J. Pedlosky, 2000: Climate variability induced by anomalous buoyancy forcing in a multilayer model of the ventilated thermocline. *J. Phys. Oceanogr.,* **30,** 3009–3021.

Kobashi, F., and H. Kawamura, 2001: Variation of sea surface height at periods of 65–220 days in the subtropical gyre of the North Pacific. *J. Geophys. Res.,* **106,** 26 817–26 831.

Lumpkin, C. F., 1998: Eddies and currents of the Hawaiian Islands. Ph.D. dissertation, University of Hawaii at Manoa, 281 pp.

Luyten, J. R., J. Pedlosky, and H. Stommel, 1983: The ventilated thermocline. *J. Phys. Oceanogr.,* **13,** 292–309.

Pedlosky, J., 1996: *Ocean Circulation Theory.* Springer, 453 pp.

——, L. J. Pratt, M. A. Spall, and K. R. Helfrich, 1997: Circulation around islands and ridges. *J. Mar. Res.,* **55,** 1199–1251.

Qiu, B., D. Koh, C. Lumpkin, and P. Flament, 1997: Existence and formation mechanism of the North Hawaiian Ridge Current. *J. Phys. Oceanogr.,* **27,** 431–444.

Rhines, P. B., and W. R. Young, 1982: A theory of the wind-driven circulation. I. Mid-ocean gyres. *J. Mar. Res.,* **40** (Suppl.), 559–596.

Roden, G. I., 1998: Upper ocean thermohaline, oxygen, nutrient, and flow structure near the date line in the summer of 1993. *J. Geophys. Res.,* **103,** 12 919–12 939.

Stammer, D., 1998: On eddy characteristics, eddy transports, and mean flow properties. *J. Phys. Oceanogr.,* **28,** 727–739.

Stanton, B., D. Roemmich, and M. Kosro, 2001: A shallow zonal jet south of Fiji. *J. Phys. Oceanogr.,* **31,** 3127–3130.

Talley, L. D., 1985: Ventilation of the subtropical North Pacific: The shallow salinity minimum. *J. Phys. Oceanogr.,* **15,** 633–649.

Wajsowicz, R. C., 1993: The circulation of the depth-integrated flow around an island with application to the Indonesian throughflow. *J. Phys. Oceanogr.,* **23,** 1470–1484.

Webb, D. J., 2000: Evidence for shallow zonal jets in the South Equatorial Current region of the Southwest Pacific. *J. Phys. Oceanogr.,* **30,** 706–720.

White, W., and A. E. Walker, 1985: The influence of the Hawaiian Archipelago upon the wind-driven subtropical gyre in the western North Pacific. *J. Geophys. Res.,* **90,** 7061–7074.

Xie, S.-P., W. T. Liu, Q. Liu, and M. Nonaka, 2001: Far-reaching effects of the Hawaiian Islands on the Pacific ocean-atmosphere system. *Science,* **292,** 1953–2204.